

See discussions, stats, and author profiles for this publication at: <https://www.researchgate.net/publication/5583348>

X-ray crystal structure and magnetic and photophysical properties of novel Copper(II) N-oxide adduct [(4-MPyO)(2)(CuCl2)(2)(H2O)(C2H5OH)] (4-MPyO=4-(4-methoxystyryl)pyridine N-oxid...

ARTICLE in INORGANIC CHEMISTRY · APRIL 2008

Impact Factor: 4.76 · DOI: 10.1021/ic701413m · Source: PubMed

CITATIONS

9

READS

62

7 AUTHORS, INCLUDING:



Yakov Nizhnik

Bioo Scientific Corp.

33 PUBLICATIONS 124 CITATIONS

SEE PROFILE



Irena Deperasińska

Institute of Physics of the Polish Academy ...

61 PUBLICATIONS 290 CITATIONS

SEE PROFILE



Korabik Maria

University of Wrocław

58 PUBLICATIONS 513 CITATIONS

SEE PROFILE

X-ray Crystal Structure and Magnetic and Photophysical Properties of Novel Copper(II) *N*-Oxide Adduct [(4-MPyO)₂(CuCl₂)₂(H₂O)(C₂H₅OH)] (4-MPyO = 4-(4-Methoxystyryl)pyridine *N*-Oxide)

Yakov P. Nizhnik,^{*,†} Anna Szemik-Hojniak,^{*,‡} Irena Deperasińska,[§] Lucjan B. Jerzykiewicz,[‡] Maria Korabik,[‡] Marek Hojniak,[‡] and Vladimir P. Andreev[†]

Department of Molecular Biology, Biological and Organic Chemistry, Petrozavodsk State University, pr. Lenina 33, 185910 Petrozavodsk, Republic Karelia, Russia, Faculty of Chemistry, University of Wrocław, Joliot-Curie 14 st, 50-383 Wrocław, Poland, and Institute of Physics, Polish Academy of Sciences, Al. Lotników 32/46, 02-668 Warsaw, Poland

Received July 16, 2007

A new mixed adduct, (4-MPyO)₂(CuCl₂)₂(H₂O)(C₂H₅OH) [where 4-MPyO is the 4-(4-methoxystyryl)pyridine *N*-oxide], was obtained for the first time. It has been characterized by X-ray studies, IR, electronic absorption, and emission spectra, lifetime measurements, and variable-temperature magnetic susceptibility measurements in the range 80–300 K. The single-crystal X-ray diffraction shows that the geometry around both of the copper(II) ions can be described as a tetragonal pyramid with a trapezoidal base at the corners of which are two oxygen atoms of *N*-oxide and two chlorine atoms. The oxygen atoms of either water or ethanol are at the apex of the pyramid. Besides that, two molecules of the adduct form a double-hydrogen-bonded superdimer in which they are connected to each other through hydrogen bonds of the O—H...Cl type as formed between the chlorine atoms and ethanol molecule (Cl...O 3.22 Å). The copper(II) atoms are antiferromagnetically coupled within a dimeric unit, and a singlet–triplet separation of 2*J* value (1100 cm^{−1}) is greater than the value expected from Hatfield's rule for the bridging angles Cu—O—Cu equal 108.9° and 110.2°. By means of the PM3-calculated values of vertical excitation energies, the ligand-to-metal charge-transfer (LMCT) and the metal-to-ligand charge-transfer transitions in the unresolved experimental absorption spectra of **1** have been revealed. From the large Stokes shift value of emission spectra in solvents of different polarity (more than 6500 cm^{−1} in acetonitrile), the charge-transfer (CT) nature of the emissive (LMCT) state of **1** has been concluded. Biexponential decay of the excited complex in acetonitrile and frozen propanol suggests that the two different CT conformers (0.8, 4.12 ns and 1.99, 15.2 ns, respectively) are present in the excited state in solution while only one CT form is indicated by a monoexponential decay (9.0 μs) in the solid.

Introduction

The practical interest in heteroaromatic *N*-oxides is caused first of all by the fact that many of them show biological activity¹ and extraction properties.² Among *N*-oxides, there are the substances possessing carcinogenic, cancerostatic, mutagenic, insecticidal, herbicidal, fungicidal, anticonvulsant, analgesic and plant-growing properties. On the other hand,

in vivo the heteroaromatic *N*-oxides both of endogenic (which can be formed in living organisms from corresponding heterocycles)³ and of exogenic origin can be the active components of donor–acceptor complexes. Thus, the *N*-oxides of 2-*n*-nonyl- and 2-*n*-heptyl-4-hydroxyquinolines synthesized by *Pseudomonas* bacteria can form complexes

* To whom correspondence should be addressed. E-mail: yakov_nizhnik@mail.ru (Y.P.N.), anias@wchuw.chem.uni.wroc.pl (A.S.-H.).

[†] Petrozavodsk State University.

[‡] University of Wrocław.

[§] Polish Academy of Sciences.

(1) Albin, A.; Pietra, S. *Heterocyclic N-Oxides*; CRC Press: Boca Raton, FL, 1991.

(2) Ejaz, M. *Sep. Sci.* **1975**, *10*, 425–446.

(3) (a) Kanou, M.; Saeki, K.; Kato, T.; Takahashi, K.; Mizutani, T. *Fundam. Clin. Pharmacol.* **2002**, *16*, 513–517. (b) Fukuwatari, T.; Wada, H.; Sasaki, R.; Shibata, K. *Biosci. Biotechnol. Biochem.* **2004**, *68*, 44–50.

(4) (a) Smirnova, I. A.; Hagerhall, C.; Konstantinov, A. A.; Hederstedt, L. *FEBS Lett.* **1995**, *359*, 23–26. (b) Furbacher, P. N.; Girvin, M. E.; Cramer, W. A. *Biochemistry* **1989**, *28*, 8990–8998.

(5) Volkova, T. O.; Nemova, N. N. *Molecular Mechanisms of Apoptosis of Leukemic Cells*; Nauka: Moscow, 2006.

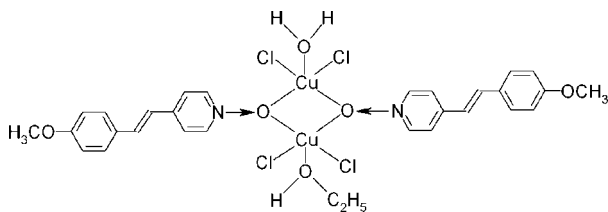


Figure 1. Formula of complex I.

with haem-containing proteins cytochromes, inhibiting the electron transport in membranes of bacteria, mitochondria, and chloroplasts.⁴

It has been recently found out that styryl derivatives of pyridine and quinoline *N*-oxides have apoptogenic, cytotoxic, and antiproliferative effects on human erythromyeloleukemic cells of line K562 and can induce their erythroid differentiation.⁵ Moreover, these compounds can exert influence on redox processes by forming a complex of the protein that can participate in apoptosis processes: cytochrome *c*, which also can induce chemical transformations of these *N*-oxides.

Heterocyclic *N*-oxides forming a complex with metal ions can be extragents for transition metals, lanthanoids, and actinoids.⁶ Thus, it has been recently established that 4-(4-methoxystyryl)pyridine *N*-oxide (4-MPyO) has larger extractive power for copper(II) than tributyl phosphate, which is usually used.⁷

Both biological activity and extractional properties are connected with complexation of *N*-oxide. Hence, all of these facts have initiated our investigations of *N*-oxide coordination with some types of electron acceptors. In this paper, we report on the preparation and properties of a copper dimer (Figure 1), which is the solvate of the complex of 4-MPyO with copper dichloride: [bis(μ_2 -4-(4-methoxystyryl)pyridine *N*-oxide- κ^O)-(aqua- κ^O)-(ethanol- κ^O)tetrachlorodicopper(II)], designated here as complex I.

Generally, the mutual interaction of two metal centers may lead to specific chemical and physical properties of the coordination compound.⁸ A great deal of attention has been focused on binuclear copper complexes⁹ that likely bind to cations of other heavy metals (Mn^{2+} , Fe^{2+} , Co^{2+} , Ni^{2+} , Ag^+ , Cd^{2+} , Hg^{2+} , and Pb^{2+}) and may be used as ratiometric fluorescent probes to investigate various biomolecules or enzyme activities.¹⁰ In order to be used as the fluorescence probes, their photophysical characteristics should be recognized.

Copper complexes, because of biologically accessible redox potentials, are also often used as reagents for selective cleavage and for characterization of the dynamics of nucleic acids.¹¹ They are effective as well as fluorescent sensors for monitoring of the metal ion concentration in biological

samples.¹² Recently, fluorescence studies on the copper(II) complexes of 3-hydroxy-3-phenyl-1-*o*-carboxyphenyltriazene¹³ and of the modified fluorescein dyes¹⁴ were undertaken. These complexes fluoresce at about 400 and 600 nm, respectively, while their emission is mainly associated with the ligand-to-metal charge-transfer (LMCT) transitions involving π^* orbitals of ligand and $d\pi$ orbitals of the Cu^{2+} ion. Both systems could be used as effective fluorescence sensor molecules for environmental and biological applications.

The charge-transfer (CT) spectra of copper(II) complexes were discussed in terms of the optical electronegativities of the ligand and metal.¹⁵ It was stated that copper-to-ligand CT transitions (MLCT) may only be possible provided that ligands have empty available orbitals and ligand optical electronegativities are smaller than 2. This is the case for pyridine *N*-oxides, whose electronegativities are around 1.0 and their π^* orbitals are accessible.¹⁶

With the exception of the purposes presented above, our aim is to check the nature of the emissive state of the copper dimer I in different media, i.e., in strongly polar and aprotic acetonitrile, in glassy (77 K) protic and less polar *n*-propanol, as well as in the solid phase to avoid solvation effects.

Experimental Section

Preparation of *N*-Oxides. 4-Methylpyridine *N*-oxide was synthesized by the method of Ochiai¹⁷ from 4-methylpyridine by peroxide oxidation in acetic acid. Yield: 89%. Mp: 185 °C (from ethanol).

4-(4-Methoxystyryl)pyridine *N*-oxide was prepared as reported¹⁸ by condensation of 4-methylpyridine *N*-oxide and 4-methoxybenzaldehyde in 10% potassium methylate in methanol upon boiling for 3 h. The obtained substance was recrystallized from ethanol. Yield: 70%. Mp: 159 °C.

Preparation of Complex I. Complex I was prepared by mixing solutions of 4-(4-methoxystyryl)pyridine (0.1135 g, 0.5 mmol) and $\text{CuCl}_2 \cdot 2\text{H}_2\text{O}$ (0.0855 g, 0.5 mmol) in 96% ethanol. The black complex $[(4\text{-MPyO})_2(\text{CuCl}_2)_2]$ crystallized immediately. The solution containing that complex was left standing for 1 month until full evaporation of the solvent occurred. Then the product was washed with a small quantity of ethanol (on 0.5 mL, two times) and dried in air. A brownish-maroon crystal powder was obtained. Calcd for $\text{C}_{30}\text{H}_{34}\text{Cl}_4\text{Cu}_2\text{N}_2\text{O}_6$: C, 45.76; H, 4.35; N, 3.56; Cl, 18.01. Found: C, 45.89; H, 4.15; N, 3.48; Cl, 18.14.

X-ray Structure Determination and Refinement. A crystal suitable for X-ray diffraction determination was grown from ethanol as mentioned above. Brownish-maroon crystals in the form of red blocks appeared after a few days.

Intensity data collection was carried out on a Kuma KM4 κ -axis diffractometer equipped with a CCD camera and an Oxford cryosystem. All data were corrected for Lorentz and polarization

- (6) (a) Nash, K. L.; Lavallette, C.; Borkowski, M.; Paine, R. T.; Gan, X. *Inorg. Chem.* **2002**, *41*, 5849–5858. (b) Bond, E. M.; Engelhardt, U.; Deere, T. P.; Rapko, B. M.; Paine, R. T. *Solvent Extr. Ion Exch.* **1998**, *16*, 967–983.
- (7) Andreev, V. P.; Tunina, S. G. *Zh. Obshch. Khim (Russian J. Gen. Chem.)* **2000**, *70*, 600–603.
- (8) Lehn, J. M.; Kneisel, O.; Baum, G.; Fenske, D. *Angew. Chem., Int. Ed. Engl.* **1966**, *35*, 1838–1840.
- (9) Spek, S.; Haasnoot, J. G.; Reedijk, J. *Eur. J. Inorg. Chem.* **2003**, 671–677.
- (10) Komatsu, K.; Kikuchi, K.; Kojima, H.; Urano, Y.; Nagano, T. *J. Am. Chem. Soc.* **2005**, *127*, 10197–10204.

- (11) Pogozelski, W. K.; Tullius, T. D. *Chem. Rev.* **1998**, *98*, 1089–1107.
- (12) Tu, C.; Shao, Y.; Gan, N.; Xu, G.; Gou, Z. *Inorg. Chem.* **2004**, *43*, 4761–4766.
- (13) Ressalan, S.; Iyer, C. S. P. *J. Lumin.* **2005**, *111*, 121–129.
- (14) Mokhir, A.; Kiel, A.; Herten, D.-P.; Kraemer, R. *Inorg. Chem.* **2005**, *44*, 5661–5666.
- (15) Jorgensen, C. K. *Absorption Spectra and Chemical Bonding in Complexes*; Pergamon Press: Oxford, U.K., 1962.
- (16) Byers, W.; Fa-Chun Chou, B.; Lever, A. B. P.; Parish, R. V. *J. Am. Chem. Soc.* **1969**, *91*, 1329–1333.
- (17) Ochiai, E. *J. Org. Chem.* **1953**, *18*, 534–551.
- (18) Brink, C. v. d. M.; de Jager, P. J. *Tydskr. Natuurwet.* **1963**, *3*, 74–80.

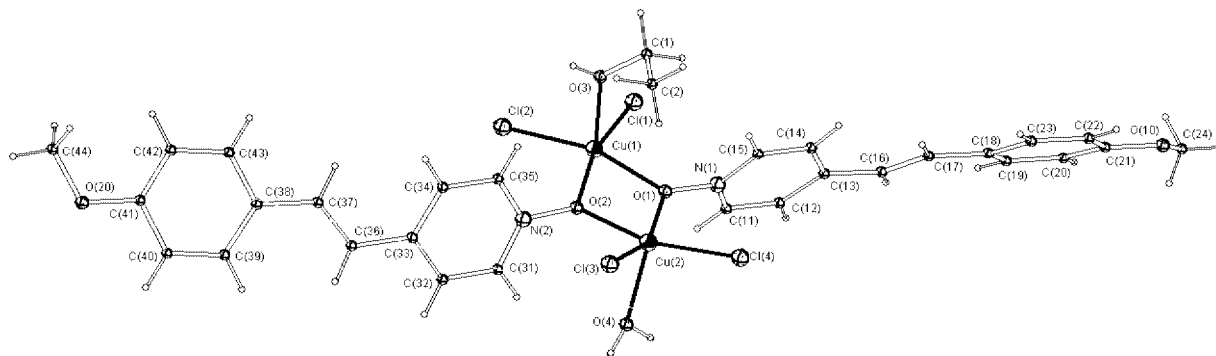


Figure 2. View of the [(4-MPyO)₂(CuCl₂)₂(H₂O)(C₂H₅OH)] unit.

Table 1. Crystal Data and Structure Refinement

compound	[bis(μ ₂ -4-(4-methoxystyryl)pyridine <i>N</i> -oxide-κ ^{O,O})-(aqua-κ ^O)(ethanol-κ ^O)-tetrachlorodicopper(II)]
chemical formula	C ₃₀ H ₃₄ Cl ₄ Cu ₂ N ₂ O ₆
MW	787.47
λ(Mo Kα) (Å)	0.710 73
<i>T</i> (K)	100(1)
space group	<i>P</i> 2 ₁ / <i>c</i>
cryst syst	monoclinic
unit cell dims	
<i>a</i> (Å)	13.467(5)
<i>b</i> (Å)	16.005(5)
<i>c</i> (Å)	14.949(5)
α (deg)	90.000(5)
β (deg)	93.839(5)
γ (deg)	90.000(5)
<i>V</i> (Å ³)	3214.9(19)
<i>Z</i>	4
<i>D_c</i> (Mg/m ³)	1.627
reflns observed <i>I</i> > 2σ(<i>I</i>)	1608
reflns measd/indep	24 340/7490
diffractometer/scan	Kuma KM-4 CCD/ω
max cryst dims (mm)	0.253 × 0.184 × 0.143
θ _{max} (deg)	28.05
range of <i>h</i> , <i>k</i> , <i>l</i>	−15/17; −20/21; −16/19
GOF	0.972
R1 = Σ(<i>F_o</i> − <i>F_c</i>)/Σ(<i>F_o</i>)	0.0353
wR2 = {Σ[<i>wF_o</i> ² − <i>F_o</i> ²]/Σ[<i>w(F_o</i> ²)]} ^{1/2}	0.0656
largest diff peak and hole (e [−] Å ^{−3})	0.752 and −0.373

effects. Data reduction and analysis were carried out with the Kuma diffraction programs.¹⁹ The structure was solved by direct methods and refined by the full-matrix least-squares method on *F*² data using the *SHELXTL* (version 5.1) program.²⁰ The X-ray crystal structure of **I** is presented in Figure 2, and corresponding experimental details are summarized in Table 1.

Spectral Measurements. IR spectra in the range 4000–100 cm^{−1} were recorded with a Bruker IFS-66/S spectrometer in KBr pellets: ν_{max}/cm^{−1} 1253s (ν_{N–O}), 1204s (ν_{N–O}), 840m (δ_{N–O}), 303s (ν_{Cu–Cl}).

The reflectance absorption spectrum was recorded with a Cary 5 spectrophotometer equipped with a reflectance setup.

Absorption spectra in solution were performed in acetonitrile and *n*-propanol solutions on a Cary 50 spectrophotometer.

Steady-state luminescence spectra were performed at room temperature in the solid state and in an acetonitrile solution as well as in frozen (77 K) *n*-propanol. The solvents for both absorption and luminescence spectra were of spectral grade, and acetonitrile was additionally dried with molecular sieves prior to use.

Luminescence spectra were recorded on a FSL920 combined fluorescence lifetime and steady-state spectrometer (Edinburgh

Instruments Ltd., Edinburgh, U.K.) using as the excitation source a Xe900 450-W steady-state xenon lamp (ozone-free) with a computer-controlled excitation shutter and with a spectral bandwidth of ≤5 nm for both excitation and emission. Luminescence was detected using a red-sensitive (185–850 nm) single-photon-counting photomultiplier tube (Hamamatsu R928) in Peltier-cooled housing. Luminescence spectra were corrected for the wavelength-dependent response of the detection system. The Universal sample chamber was equipped with a single-position right-angle geometry sample holder (front-face geometry for the solid sample), a detector shutter interlock, an iris diaphragm to attenuate the signal level, and a reference detector for spectral correction of excitation files and with an integrated controller to control and monitor spectrometer operation. Monochromatization of light was ensured by TMS300 300-mm focal excitation and emission Czerny Turner monochromators. They had computer-controlled triple-grating turrets and slits. Stray light suppression was greater than 1:10,⁵ the linear dispersion was 1.8 nm/mm, and the slits were adjustable from 0.05 to 18 nm in 0.01 nm steps (grating-dependent).

Time-Resolved Luminescence Spectroscopy. Luminescence decay curves for an acetonitrile solution and frozen (77 K) *n*-propanol were recorded using the time-correlated single-photon-counting (TCSPC) option of the FSL920 setup (Edinburgh Instruments Ltd., Edinburgh, U.K.). Excitation was provided by an nF900 nitrogen-filled nanosecond flash lamp under computer control, with typical pulse widths of 1 ns, a pulse repetition rate typically of 40 kHz, and the possibility of measuring decays from 100 ps to 50 μs.

Data acquisition ensured a PC Plug-in Card model TCC900 with a maximum count rate of 3 MHz, time channels per curve of up to 4096, and a minimum time per channel of 610 fs. A Hamamatsu R928 in Peltier-cooled housing was used as the detector.

Luminescence decay curves for the solid phase of complex **I** were recorded using the microsecond TCSPC option of the FLS920 setup (Edinburgh instruments Ltd., Edinburgh, U.K.). Excitation was provided by a μF900 microsecond xenon flash lamp under computer control with pulses of 1.5–3 μs, an average power of >60 W up to 100 Hz, and the possibility of measuring decays from 400 ns to 10 s. The multichannel scaling mode required a TCC900 fast-counter PC Plug-in Card. The PG900 microsecond photomultiplier gating option was used to fix the gate width and gate delay, and a Hamamatsu R928 in Peltier-cooled housing was used as the detector.

Theoretical Calculations. Ground-state optimization of **I** by means of ab initio or density functional theory methods on a high level of calculations was not possible because of its large dimen-

(19) Oxford Diffraction Ltd. *CrysAlis CCD and CrysAlisRED*, version 1.171; Oxford Diffraction Ltd.: Abingdon, Oxfordshire, England, 2003.

(20) Sheldrick, G. M. *SHELXTL*, version 5.1; Bruker AXS Inc.: Madison, WI, 1998.

Table 2. Internuclear Distances (Å) in Complex **I**

Cu(1)–Cu(2)	3.293(1)	O(2)–N(2)	1.359(2)
Cu(1)–Cl(1)	2.232(1)	N(1)–C(11)	1.349(3)
Cu(1)–Cl(2)	2.250(2)	N(1)–C(15)	1.347(3)
Cu(1)–O(1)	2.004(2)	N(2)–C(31)	1.345(3)
Cu(1)–O(2)	2.012(2)	N(2)–C(35)	1.344(3)
Cu(1)–O(3)	2.280(2)	O(10)–C(21)	1.367(3)
Cu(2)–Cl(3)	2.232(1)	O(10)–C(24)	1.431(3)
Cu(2)–Cl(4)	2.225(1)	O(20)–C(41)	1.380(3)
Cu(2)–O(1)	2.044(2)	O(20)–C(44)	1.448(3)
Cu(2)–O(2)	2.003(2)	C(16)–C(17)	1.347(3)
Cu(2)–O(4)	2.238(2)	C(36)–C(37)	1.343(3)
O(1)–N(1)	1.360(2)	C(1)–C(2)	1.502(4)

sions. Instead, semiempirical PM3²¹ calculations of excited energies and the oscillator strength were performed. These calculations were based on the X-ray structure of **I**.

Magnetic Measurements. Magnetization measurements in the temperature range 1.8–300 K were carried out on powdered samples of complex **I**, at a magnetic field of 0.5 T, using a Quantum Design SQUID magnetometer (type MPMS-XL5). Corrections for diamagnetism of the constituting atoms were calculated using the Pascal constants;²² the value of $60 \times 10^{-6} \text{ cm}^3 \text{ mol}^{-1}$ was used as the temperature-independent paramagnetism of the copper(II) ion. The effective magnetic moments were calculated from the expression (1):

$$\mu_{\text{eff}} = 2.83 \sqrt{\chi_{\text{m}}^{\text{corr}} T} \quad \mu_{\text{B}} \quad (1)$$

Results and Discussion

The obtained complex **I** can be classified based on work by Watson²³ as the adduct of the 1:1 complex. CH₃OH, H₂O, dimethyl sulfoxide (DMSO), and *N,N*-dimethylformamide are of common occurrence in these cases. Complex **I**, containing two different extra ligands (C₂H₅OH and H₂O), has been prepared for the first time from 96% ethanol. Surprisingly, the water participates upon complexation despite a prominent ethanol excess. It should be noted that the complex [(4-MPyO)₂(CuCl₂)₂] is formed immediately after mixing components' solutions in 96% ethanol.²⁴ However, as we found out, this complex adds water and ethanol upon standing over time in a mother solution, forming complex **I**. We consider that probably the first complex is formed under kinetic control, and then complex **I** is formed under thermodynamic control.

An almost analogous phenomenon was observed by Estes and Hodgson;²⁵ it has been noted that first in ethanol formed precipitate [(PyO)₂(CuCl₂)₂] was dissolved upon the addition of water, but then crystals of adduct [(PyO)₂(CuCl₂)₂(H₂O)₂] were obtained after the solution was allowed to stand for a few days.

X-ray Crystal Structure. Complex **I** consists of binuclear units; its structure is shown in Figure 2, and selected geometrical parameters are given in Tables 2 and 3.

The geometry around the copper atoms can be described as a tetragonal pyramid with a trapezoidal base, at the corners

Table 3. Internuclear Angles (deg) in Complex **I**

Cu(1)–O(1)–Cu(2)	108.86(7)	Cl(3)–Cu(2)–O(4)	97.54(6)
Cu(1)–O(2)–Cu(2)	110.24(7)	Cl(4)–Cu(2)–O(4)	100.79(5)
O(1)–Cu(1)–O(2)	70.04(6)	Cu(1)–O(1)–N(1)	124.99(14)
O(1)–Cu(2)–O(2)	69.43(6)	Cu(2)–O(1)–N(1)	125.97(13)
O(1)–Cu(1)–Cl(1)	94.81(5)	Cu(1)–O(2)–N(2)	125.12(13)
O(1)–Cu(2)–Cl(4)	95.06(5)	Cu(2)–O(2)–N(2)	124.30(14)
O(2)–Cu(1)–Cl(2)	95.47(5)	C(11)–N(1)–C(15)	122.3(2)
O(2)–Cu(2)–Cl(3)	93.86(5)	C(31)–N(2)–C(35)	122.3(2)
O(1)–Cu(2)–O(4)	99.46(7)	C(13)–C(16)–C(17)	122.8(2)
O(2)–Cu(2)–O(4)	88.95(7)	C(16)–C(17)–C(18)	128.6(2)
O(1)–Cu(1)–O(3)	98.84(7)	C(33)–C(36)–C(37)	122.7(2)
O(2)–Cu(1)–O(3)	92.99(7)	C(36)–C(37)–C(38)	128.3(2)
Cl(1)–Cu(1)–O(3)	97.42(5)	C(21)–O(10)–C(24)	117.84(19)
Cl(2)–Cu(1)–O(3)	91.54(5)	C(41)–O(20)–C(44)	117.62(18)

of which are two bridging oxygen atoms of *N*-oxide, O(1) and O(2), and two chlorine atoms. The oxygen atoms of either water or ethanol are at the apex of the pyramid. The basal atoms are almost coplanar. In the case of water as the axial ligand, the atoms O(1) and Cl(3) are lying at 0.099 and 0.069 Å, respectively, below the least-squares plane through the four atoms and O(2) and Cl(4) are lying at 0.101 and 0.067 Å, respectively, above it. In the case of the pyramid with ethanol oxygen atom as its apex, the atoms O(1), Cl(1), O(2), and Cl(2) are −0.016, +0.011, +0.016, and −0.011 Å, respectively, from their plane.

The copper atom connected with water lies within the pyramid at a distance of 0.261 Å from the basal plane. In the case of the other copper atom (which is connected to the ethanol molecule), this distance is 0.190 Å. The larger value in the first case is, probably, due to the fact that water forms a hydrogen bond, and this can pull its molecule a bit out. Literature data are 0.231 Å for bis[dichloroaquo(pyridine *N*-oxide)copper(II)].²⁵

The apical ligands (water and ethanol) are trans with respect to the plane formed by the chlorine atoms and bridging oxygens. The Cu–O(4) distance of 2.238 Å and the Cu–O(3) distance of 2.280 Å are normal for apical coordination to copper (in the anorthic polymorph bis[dichloroaquo(pyridine *N*-oxide)copper(II)], the Cu–OW distance²⁵ is 2.336 Å; in the monoclinic polymorph form, this distance²⁶ is 2.267 Å). The Cu(1)–O(1)–Cu(2) and Cu(1)–O(2)–Cu(2) angles of 108.86° and 110.24°, respectively, and the Cu(1)–Cu(2) separation of 3.293 Å fall in the ranges observed for other complexes.²⁵ The Cu(1)–Cu(2) distance is consonant with the mechanism of superexchange through oxygen orbitals on the basis of magnetic susceptibility data as proposed by Hatfield and Paschal.²⁷ The Cu–O(bridging) distances (2.004, 2.012, 2.003, and 2.044 Å) and Cu–Cl distances (2.232, 2.250, 2.232, and 2.225 Å) are similar to those in other complexes of this type. Thus, in the case of bis[dichloroaquo(pyridine *N*-oxide)copper(II)], Cu–O(bridging) distances are 1.996 and 2.013 Å and Cu–Cl distances are 2.216 and 2.221 Å.²⁵ An analogous complex with DMSO, di-μ-(pyridine *N*-oxide)bis[dichloro(dimethyl sulfoxide)cop-

(21) Dewar, M. J. S.; Zoebish, E. G.; Healy, E. F.; Stewart, J. J. P. *J. Am. Chem. Soc.* **1985**, *107*, 3902–3909.

(22) König, E. *Magnetic Properties of Coordination and Organometallic Transition Metal Compounds*; Springer-Verlag: Berlin, 1966.

(23) Watson, W. H. *Inorg. Chem.* **1969**, *8*, 1879–1886.

(24) Andreev, V. P.; Nizhnik, Y. P.; Tunina, S. G.; Belashev, B. Z. *Khim. Geterotsikl. Soedin. (Chem. Heterocycl. Compd., Latvia)* **2002**, 634–641.

(25) Estes, E. D.; Hodgson, D. J. *Inorg. Chem.* **1976**, *15*, 348–351.

(26) Gawron, M.; Palenik, R. C.; Palenik, G. J. *Acta Crystallogr., Sect. C* **1988**, *44*, 168–170.

(27) Hatfield, W. E.; Paschal, J. S. *J. Am. Chem. Soc.* **1964**, *86*, 3888–3889.

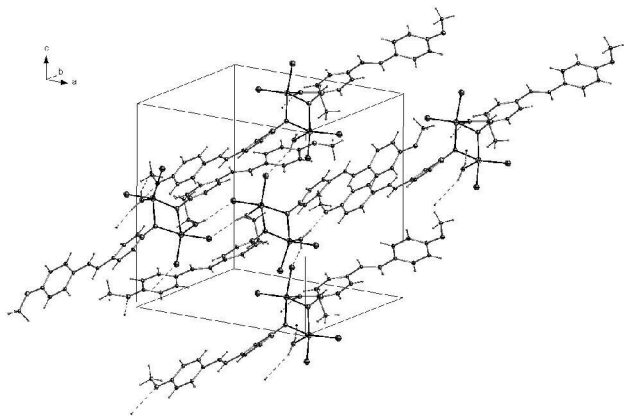


Figure 3. Crystal packing of complex **I**. Dotted lines show the hydrogen bonds.

per(II)], has values similar to those of Cu–O(bridging) and Cu–Cl distances (2.046, 2.260, and 2.242 Å, respectively).²⁸

The dihedral angles between bridging and pyridine planes of 75.04° (ligand 1) and 72.57° (ligand 2) are normal (72.44°,²⁹ 70.01°,³⁰ and 69.72°³¹ in bis[dichloro(pyridine *N*-oxide)copper(II)]; 87.59°,²⁵ 86.95°,³² and 87.42°²⁶ in bis[dichloroaquo(pyridine *N*-oxide)copper(II)]). It should be noted that usually two pyridine rings lie in the same plane. However, in contrast to known complexes, the pyridine rings in complex **I** form a torsion angle of 32.49°.

Two molecules of complex **I** form a double-hydrogen-bonded dimer in which they are connected to each other by O–H···Cl types of hydrogen bonds between chlorine atoms and an ethanol molecule (Cl···O 3.22 Å; Figure 3). Similar dimers are formed in the case of dichloro[(5-(3,3-dimethyl-1-triazenyl)imidazole-4-carboxamido)methanol]copper(II) (Cl···O 3.246 Å),³³ tetrachloro[(μ₂-2,4,6-tris(2-pyridyl)-1,3,5-triazine)(methanol)]dicopper(II) (Cl···O 3.011 Å),³⁴ chloro[(2,6-bis((3,5-dimethylpyrazol-1-yl)methyl)pyridine)methanol]copper(II) tetrafluoroborate (Cl···O 3.108 Å),³⁵ catena(dibromo[(μ₂-2,11-dithia[3.3]paracyclophane)ethanol]copper(II)) (Br···O 3.329 Å),³⁶ and dichloro[ethanolatobis(4-amino-(*N*-2-thiazolyl)benzenesulfonamide-*N*)]copper(II) (Cl···O 3.126 Å).³⁷ Moreover, few examples of formation of the polymer in the same way are known. This situation can be found in the case of a water solvate of the complex of copper dichloride with pyridine *N*-oxide: bis(dichloroaqua(μ₂-pyri-

dine *N*-oxide)copper(II). In this case, weak hydrogen bonds between chlorine and oxygen atoms of water (Cl···O 3.315 Å for anorthic³² and 3.214 and 3.244 Å for monoclinic²⁶ modifications) form the polymer structure of the complex that is demonstrated in Figure 3.

Moreover, the water molecules form the O–H···O type hydrogen bonds with oxygen of the CH₃O group of another dimeric unit (O···O 2.761 Å), forming in this way an infinite chain of dimers. It should be noted that only one ligand molecule in the binuclear complex forms a hydrogen bond with water; the second CH₃O group is free.

We assume that the crystal structure of the title compound could be stabilized by possible π–σ interaction³⁸ between pyridine and benzene rings of the two molecules of complex **I** as well as by stacking interactions between corresponding dimers because the distances between rings are 3.318 and 3.314 Å.

Because the molecule of complex **I** is not symmetric, two ligand molecules exhibit different bond lengths and angles. The ligand molecule with N(1) and O(1) will be denoted as “ligand 1” and, correspondingly, the second ligand with N(2) and O(2) as the “ligand 2”. The ligand molecule is a trans isomer, which is consistent with NMR and IR spectra of the free ligand. The pyridine and benzene moieties of *N*-oxide are out-of-plane: torsion angles are 21.81° (ligand 1) and 23.59° (ligand 2). Analogous “twist” is possible in the other cases: torsion angles between two rings are 26.09° and 24.96° in (*E*)-3,5,4'-trimethoxystilbene,³⁹ 13.11° in (μ₃-4-(2-(4-methoxyphenyl)ethenyl)pyridiniummethylidene)bis(μ₂-hydrido)tris(tricarbonylosmium),⁴⁰ and 30.77° in 4-(2-(4-methoxyphenyl)ethenyl)-*N*-methylpyridinium tetraphenylborate.⁴¹

Each of the pyridine moieties is almost exactly planar, with the six atoms having a mean distance of 0.015 Å (ligand 1) and 0.021 Å (ligand 2) from the least-squares plane through them; the greatest distances were 0.025 and 0.032 Å, respectively. The benzene parts of the styryl group are also planar; the mean distance was 0.005 Å and the greatest distance was 0.008 Å for both ligands. The bond lengths and angles are essentially the same as those found in other cases. The lengths of the double bonds of the styryl fragments of 1.347 Å (ligand 1) and 1.343 Å (ligand 2) are similar to those observed in 4-[4-(dimethylamino)styryl]pyridine *N*-oxide:⁴² 1.340 and 1.337 Å in stilbazole.⁴³

The distance N → O [N(1)–O(1) 1.360 Å; N(2)–O(2) 1.359 Å] should be increased in comparison with parent *N*-oxide as a consequence of the diminishing of the N → O double character upon coordination. The oxygen atoms are 0.056 Å [O(1)] and 0.121 Å [O(2)] out of the corresponding pyridine plane, and the N–O bond makes angles of 1.79°

(28) Williams, R. J.; Watson, W. H.; Larson, A. C. *Acta Crystallogr., Sect. B* **1975**, *31*, 2362–2364.

(29) Schafer, H. L.; Morrow, J. C.; Smith, H. M. *J. Chem. Phys.* **1965**, *42*, 504–508.

(30) Sager, R. S.; Williams, R. J.; Watson, W. H. *Inorg. Chem.* **1967**, *6*, 951–955.

(31) Atria, A. M.; Cortés, P.; Garland, M. T.; Baggio, R. *Acta Crystallogr., Sect. E* **2003**, *59*, 967–969.

(32) Paulson, J. A.; Krost, D. A.; McPherson, G. L.; Rogers, R. D.; Atwood, J. L. *Inorg. Chem.* **1980**, *19*, 2519–2525.

(33) Freeman, H. C.; Hutchinson, N. D. *Acta Crystallogr., Sect. B* **1979**, *35*, 2045–2050.

(34) Glaser, T.; Lügger, T.; Fröhlich, R. *Eur. J. Inorg. Chem.* **2004**, 394–400.

(35) Foster, C. L.; Kilner, C. A.; Thornton-Pett, M.; Halcrow, M. A. *Polyhedron* **2002**, *21*, 1031–1041.

(36) Yamamoto, M.; Wu, L. P.; Kuroda-Sowa, T.; Maekawa, M.; Suenaga, Y.; Munakata, M. *Inorg. Chim. Acta* **1997**, *258*, 87–91.

(37) Casanova, J.; Alzuet, G.; Borras, J.; Timoneda, J.; García-Granda, S.; Candano-Gonzalez, I. *J. Inorg. Biochem.* **1994**, *56*, 65–76.

(38) Janiak, C. *J. Chem. Soc., Dalton Trans.* **2000**, 3885–3896.

(39) Yin, Q.; Shi, Y.-M.; Liu, H.-M.; Li, Ch.-B.; Zhang, W.-Q. *Acta Crystallogr., Sect. E* **2002**, *58*, 1180–1181.

(40) Wong, W.-Y.; Wong, W.-T. *J. Organomet. Chem.* **1999**, *584*, 48–57.

(41) Li, S.-J.; Zhang, D.-Ch.; Huang, Zh.-L.; Zhang, Y.-Q.; Yu, K.-B. *Acta Crystallogr., Sect. C* **2000**, *56*, 1122–1123.

(42) Ivashevskaia, S. N.; Aleshina, L. A.; Andreev, V. P.; Nizhnik, Y. P.; Chernyshev, V. V.; Schenk, H. *Acta Crystallogr., Sect. E* **2003**, *59*, 1006–1008.

(43) Cariati, E.; Roberto, D.; Ugo, R.; Srdanov, V. I.; Galli, S.; Macchi, P.; Sironi, A. *New J. Chem.* **2002**, *26*, 13–15.

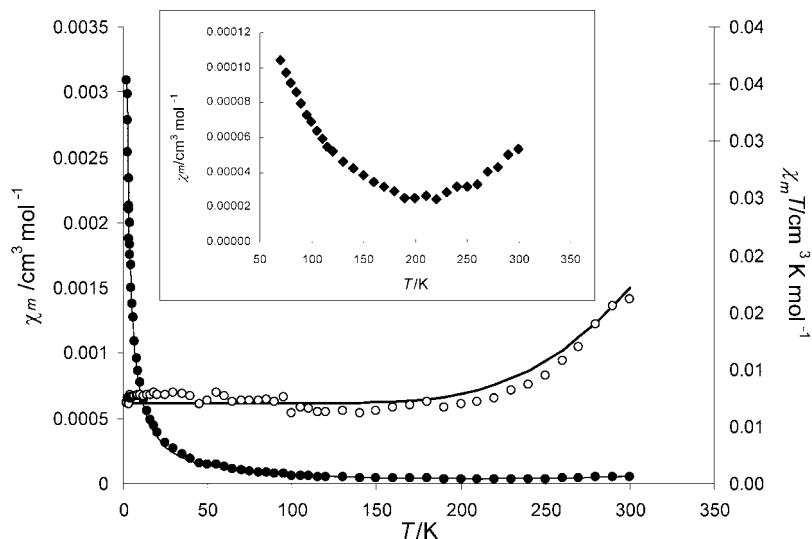


Figure 4. Plots of χ_m and $\chi_m T$ vs T for **I**. The solid line is the theoretical one (see the parameters in the text). The inset shows the temperature dependence of magnetic susceptibility in the range 80–300 K and tendency of the magnetic susceptibility to increase above 200 K.

[N(1)–O(1)] and 3.84° [N(2)–O(2)] with the ring plane (0.068 \AA and 1.96° in the case of bis(μ -quinoline *N*-oxide- $\kappa^{2O:O}$)bis[dichlorocopper(II)]).⁴⁴

The lengths C–O (1.367 and 1.380 \AA) and O–CH₃ (1.430 and 1.448 \AA) and angle C–O–C (117.63° and 117.84°) are in agreement with the literature data [1.369 and 1.424 \AA and 117.64° for (*E*)-3,5,4'-trimethoxystilbene;³⁹ 1.396 and 1.447 \AA and 115.08° in (μ_3 -4-(2-(4-methoxyphenyl)ethenyl)pyridiniummethylidyne)bis(μ_2 -hydrido)tris(tricarbonyl-osmium);⁴⁰ 1.364 and 1.422 \AA and 118.24° in 4-(2-(4-methoxyphenyl)ethenyl)-*N*-methylpyridinium tetraphenylborate⁴¹]. The C–O distance in the CH₃O group forming the hydrogen bond is increased.

Magnetic Properties. Magnetic measurements of complex **I** are presented in Figure 4 in the form of a χ_m and $\chi_m T$ vs T plot (χ_m being the corrected molar magnetic susceptibility per copper(II) and T the absolute temperature).

The $\chi_m T$ value is extremely smaller than the theoretical value [typically $0.4 \text{ cm}^3 \text{ K mol}^{-1}$ per one copper(II)] and magnetic susceptibility starts to gradually increase upon heating from 200 K. This behavior can be interpreted in terms of the singlet–triplet model⁴⁵ with considerably strong antiferromagnetic coupling. Increasing of magnetic susceptibility, below 50 K, is observed because of monomeric impurity, very often existing in a dimeric type structure of copper(II) complexes.^{45,46} The modified Bleaney–Bowers equation (eq 2) was used for the analysis of magnetic data.

$$\chi_m^{\text{corr}} = \left\{ \frac{Ng_{\text{dim}}^2 \beta^2}{3kT} [1 + 1/3(e^{-2J/kT})]^{-1} \right\} (1-x) + \left(\frac{Ng_{\text{mon}}^2 \beta^2}{4kT} \right) x \quad (2)$$

where x is the percent of monomeric impurity, $2J$ is the singlet–triplet energy gap, and other symbols have their usual

meaning. The best fit of the experimental data gave the following parameters: $J = -550 \text{ cm}^{-1}$, $x = 1.6\%$, $g_{\text{dim}} = g_{\text{mon}} = 2.15$, $R = 2.7 \times 10^{-3}$. R is the agreement factor defined in eq 3.

$$R = \sum_{i=1}^n \frac{(\chi_i^{\text{exp}} T - \chi_i^{\text{calc}} T)^2}{(\chi_i^{\text{exp}} T)^2} \quad (3)$$

It is well-known that copper(II) halides with pyridine *N*-oxides produce large magnetic exchange.⁴⁶ The singlet–triplet energy gap, $2J = -1100 \text{ cm}^{-1}$, observed for the analyzed complex **I**, is greater than the value expected from Hatfield's rule^{46,47} for bridging angles Cu–O–Cu equal to 108.9° and 110.2° . They confirm very strong antiferromagnetic coupling between copper(II) ions in dimeric units of **I**.

Spectroscopy. IR Spectra. A comparison of the IR spectrum of *N*-oxide with the spectrum of compound **I** in KBr disks (Figure 5) shows a remarkable decrease in the frequency of the N–O stretching vibrations (at 1250 cm^{-1}) upon coordination. Moreover, a new strong band at 1204 cm^{-1} appears that may be assigned to stretching vibrations of the N–O group connected to copper. The formation of a donor–acceptor bond diminishes the N–O double character and induces a shift (49 cm^{-1}) to the lower frequency region. Analogous changes were described for other complexes of *N*-oxides.^{48,49} These shifts indicate oxygen coordination. The N–O bending vibration assigned to the medium band at 840 cm^{-1} undergoes no appreciable changes upon coordination, which is in agreement with the literature data.⁴⁸ The situation with $\nu_{\text{Cu–Cl}}$ is more complex. It is known that 1:1 complexes that exhibited subnormal magnetic moments possessing binuclear oxygen-bridged structures afforded “terminal”

(46) Kato, M.; Muto, Y. *Coord. Chem. Rev.* **1988**, 92, 45–83, and references cited therein.

(47) Galy, J.; Jaud, J.; Kahn, O.; Tola, P. *Inorg. Chim. Acta* **1979**, 36, 229–236.

(48) Kida, S.; Quagliano, J. V.; Walmsley, J. A.; Tyree, S. Y. *Spectrochim. Acta* **1963**, 19, 189–199.

(49) Garvey, R. G.; Nelson, J. N.; Ragsdale, R. O. *Coord. Chem. Rev.* **1968**, 3, 375–407.

(44) Ivashevskaja, S. N.; Aleshina, L. A.; Andreev, V. P.; Nizhnik, Y. P.; Chernyshev, V. V. *Acta Crystallogr., Sect. E* **2002**, 58, 721–723.

(45) Bleaney, B.; Bowers, K. D. *Proc. R. Soc. London, Ser. A* **1952**, 214, 451–465.

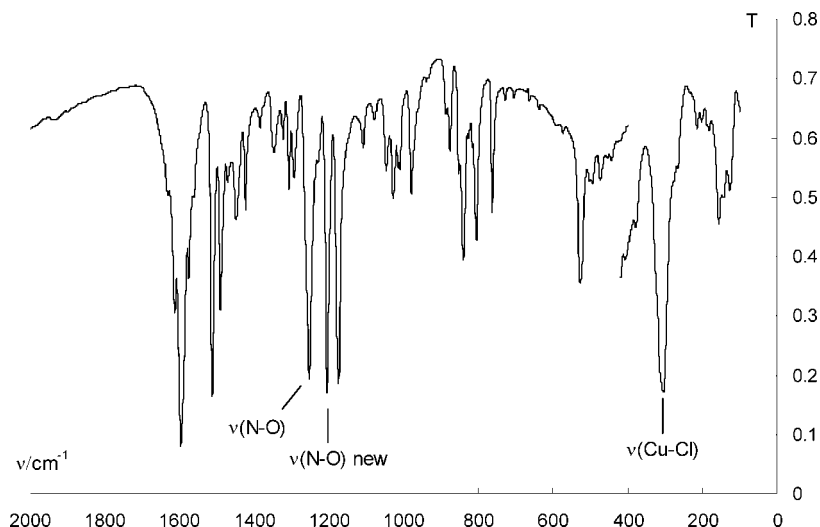


Figure 5. IR spectrum of complex **I** in KBr.

metal–chlorine stretching frequencies in the range 344–325 cm^{-1} . For the condensed compounds that show normal magnetic behavior, the maxima were shifted by 40 cm^{-1} to lower energy, occurring in the range 308–280 cm^{-1} . This shift is considered to reflect the difference between structural species containing terminal and bridging metal–chlorine bonds.⁵⁰ In the compounds with low magnetic moments and presumably oxygen-bridged structures, maxima observed at 330 and 340 cm^{-1} are assigned as terminal metal–chlorine stretching frequencies.⁵¹

In the case of complex **I**, a strong frequency band at 303 cm^{-1} appeared and can be assigned as $\nu_{\text{Me-Cl}}$. According to the literature data,⁵⁰ it has to be assigned to bridged chlorine atoms. However, according to X-ray data, complex **I** has two oxygen bridges in the molecule. Moreover, antiferromagnetism is evidence for *N*-oxide bridging, which commonly produces strong antiferromagnetism. Whyman et al.,⁵¹ upon noting that the Cu–Cl vibrational frequency in the 2:1 complex of pyridine *N*-oxide with CuCl₂ with an *N*-oxide bridge (310 and 286 cm^{-1}) is lower than that in the 1:1 complexes, suggested that entry of an additional ligand into the coordinational sphere weakens the Cu–Cl bonding, causing a reduction in the Cu–Cl stretching frequencies. Thus, in our case, the presence of two additional ligands (water and ethanol) can cause the same effect. Moreover, it should be taken into account that hydrogen bonds are formed with chlorine atoms and ethanol in dimers.

Electronic Reflectance Absorption Spectrum. The electronic diffuse reflectance spectrum of a copper dimer presented in Figure 6 exhibits a broad absorption band in the visible region with metal-centered transitions (*d*–*d*) at about 870 nm. In addition, a stronger and a very broad band, probably a superposition of LMCT and MLCT transitions, ranges from about 390 to 650 nm, with the maximum at about 404 nm.

A rough comparison of these maxima with PM3-calculated gas-phase vertical excitation energies is presented in Table 4. Likely to other transition-metal complexes, also in this dimer

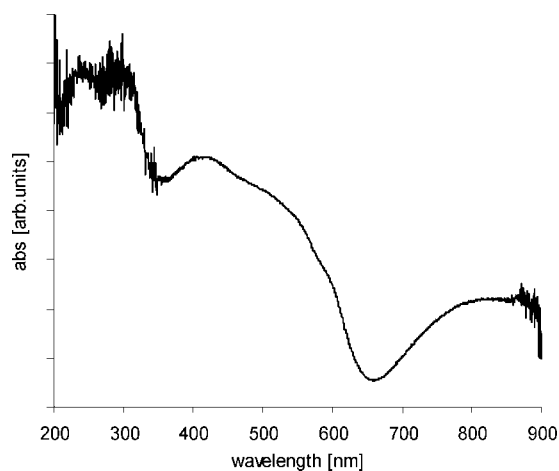


Figure 6. Reflectance spectrum of complex **I**.

the configurational mixing among an enormous number of its electronic excited states makes it exceedingly difficult to achieve a particular understanding of their properties.

It is worth noticing that an inversion of states occurs in the solid phase in comparison to the gas phase. Gas-phase-calculated MLCT and LMCT bands resulting from dominating contribution of the 125 → 126 electronic configuration for which the frontiers of HOMO–LUMO orbitals are displayed in Table 5 are located around 600 nm (638.5 and 568.3 nm).

Their excited-state dipole moment value, a parameter that is characteristic of the CT states, is increased a few times (11.31 and 8.59 D) relative to the ground state (3.57 D). On the other hand, in the solid, the lowest in energy (about 870 nm) are the metal-centered (*d*–*d*) transitions. The latter ones find their gas-phase counterparts ranging from 360 to 400 nm (Table 4). Their excited-state dipole moment does not change readily, and these transitions result mainly from 125 → 131 and from 114 → 126 electronic configurations (Table 5).

The highest calculated (289.6 nm) transition energy originates from a mixture of different ligand-centered π – π^* electronic configurations and those of the MLCT transition. It agrees with experimental transitions at 279 and 299 nm.

Room Temperature Absorption Spectra in Solution. As is demonstrated in Table 6, experimental absorption spectra

(50) Whyman, R.; Hatfield, W. E. *Inorg. Chem.* **1967**, *6*, 1859–1862.

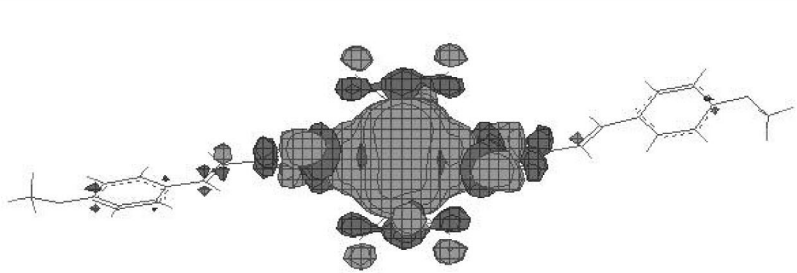
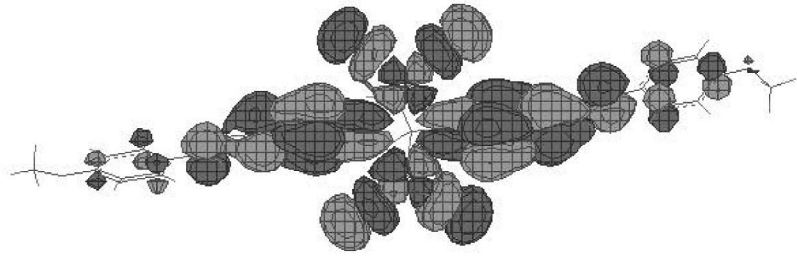
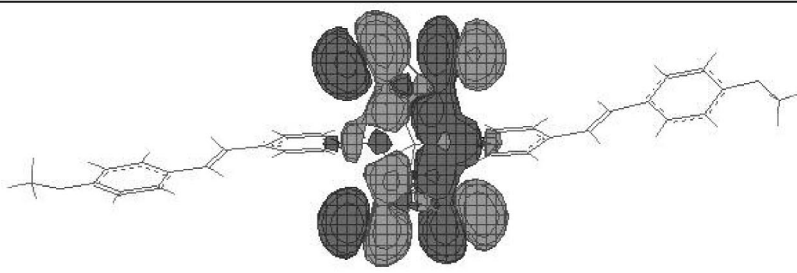
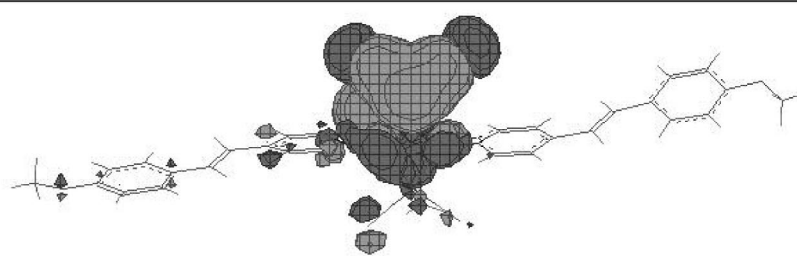
(51) Whyman, R.; Copley, D. B.; Hatfield, W. E. *J. Am. Chem. Soc.* **1967**, *89*, 3135–3141.

Table 4. PM3-Calculated Vertical Excitation Energies and Dominating Electronic Configurations Contributing to the Particular Transition of the Dimeric Form of **I** and Compared to Those in its Reflectance Spectrum ($\lambda_{\text{exp}}^{\text{Abs}}$)

$\lambda_{\text{calc}}^{\text{Abs}}/\text{nm}$	oscillator strength (<i>f</i>)	$\mu_{\text{E}}/D(\text{calc})$	electronic config	type of band (gas)	$\lambda_{\text{exp}}^{\text{Abs}}/\text{nm}$ (solid)	type of band (solid)
638.5, 568.3	0.032, 0.107	11.31, 8.59	125 \rightarrow 126	MLCT, LMCT	870	d \rightarrow d
403.2, 393.3	0.223, 0.614	1.34, 2.15	125 \rightarrow 131	MLCT	390–650	MLCT, LMCT
377.5, 355.6	0.201, 0.437	2.68, 3.58	114 \rightarrow 126	MLCT + DEC ^a	344	MLCT
289.6	0.230	5.50	111 \rightarrow 126, 110 \rightarrow 126	MLCT + DEC ^a	299, 279	MLCT

^a DEC means different (π , π^*) electronic configurations.

Table 5. Frontiers of Chosen Molecular Orbitals of the Copper Dimer: PM3 Computations (L = LUMO and H = HOMO)

L-131	
L-126	
H-125	
H-114	

of complex **I** in *n*-propanol and in acetonitrile show the first band at 358 and 355 nm, respectively.

One may easily assign both of them to the PM3-calculated MLCT band at 350 nm with a very low oscillator strength (0.0005) and with a large excited-state dipole moment of 13.62 D in comparison to the ground-state dipole moment value 3.57 D.

The two higher energy bands in acetonitrile (227 and 276 nm) also show their CT character, and the band at about 227 nm may be assigned to the calculated LMCT band at 227 nm ($f = 0.001$; $\mu = 25.24$ D), whereas the shoulder at 276 nm ($f = 0.001$; $\mu = 27.17$ D) may be assigned to the

MLCT transition. In *n*-PrOH, the two UV bands (210 and 202 nm, respectively) show a mixed (π – π^* + CT) character. Their oscillator strength (0.13 and 0.49, respectively) might be characteristic of π – π^* transitions while their dipole moments are significantly larger (9.80 and 10.80 D, respectively) than those in the ground state.

Excitation Fluorescence Spectra. It is interesting to note (Figure 7) that the room temperature excitation fluorescence spectra in *n*-PrOH and acetonitrile observed from both fluorescence maxima (429 and 460 nm in *n*-PrOH and 439 and 462 nm in acetonitrile) nicely reproduce the absorption

Table 6. Photophysical Parameters of **I**^a

solvent	$\lambda_{\text{exp}}^{\text{abs}}/\text{nm}$	$\lambda_{\text{exc}}/\text{nm}$	$\Delta E/\text{nm}$ (calc)	PM3 assignment (f , μ/D)	$\lambda_{\text{max}}^{\text{F}}/\text{nm}$	$\Delta\nu_{\text{ST}}/\text{cm}^{-1}$	τ/ns (amplitude)
<i>n</i> -PrOH (77 K)	358 210, 202	360	350 213 198	MLCT (0.0005, 13.62) $\pi-\pi^* + \text{CT}$ (0.13, 9.80) $\pi-\pi^* + \text{CT}$ (0.49, 10.8)	425	4241	1.99 (88%), 15.2 (12%)
CH ₃ CN	355 275sh 227	355	348 276	MLCT (0.0003, 16.63) CT (0.06, 27.17) CT (0.001, 25.24)	440 462	5442 6524	0.79 (91%), 4.12 (9%) 0.70 (96%), 3.59 (4%)
solid phase	404	360	398.5	MLCT (0.00, 13.94)	425 440 467 536	4241 5043	9.59 [μs] (em. 425) 9.24 [μs] (em. 467) 8.96 [μs] (em. 536)

^a For comparison purposes, the PM3-calculated values of excitation energies (ΔE), oscillator strength (f), and dipole moment vales are displayed.

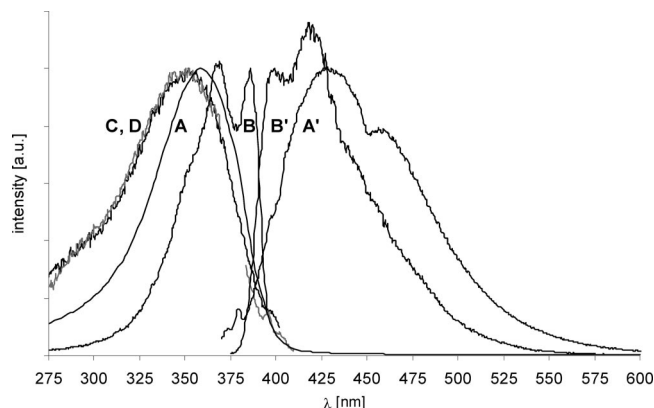


Figure 7. Absorption and fluorescence room temperature (RT) and low-temperature (77 K) spectra of **I** in *n*-PrOH: absorption-RT (A); fluorescence-RT (A'); excitation fluorescence-RT, $\lambda_{\text{obs}} = 430$ nm (C); excitation fluorescence-RT, $\lambda_{\text{obs}} = 460$ nm (D); excitation fluorescence-77 K, $\lambda_{\text{obs}} = 398$ nm (B); fluorescence-77 K (B').

spectra. Also a mirror symmetry image occurs between the absorption (or fluorescence–excitation) and the emission spectra of **I**, both at room temperature and at 77 K. These findings allow us to conclude that in the ground state there is only one stable conformation of **I**.

Further inspection of Figure 7 allows us to conclude that at 77 K a trace of the vibrational structure appears both in the excitation spectrum and in the fluorescence spectrum ($\lambda_{\text{max}} = 425$ nm) of **I**. Besides that, the lower energy fluorescence band almost disappears. This fact seems to be connected with the excited-state perpendicular conformation of **I** that is characteristic of other styryl derivatives.^{52,53} In the crystal structure of **I**, the one 4-(4-methoxystyryl)pyridine *N*-oxide subunit is perpendicular with respect to the second one, while in room temperature solutions, where all functional groups rotate, a reverse situation is also possible. A double-bumped emission band may be observed in the case of liquid propanol (429 and 460 nm) and acetonitrile (439 and 462 nm). In the glassy frozen *n*-PrOH, this movement is blocked and only a higher energy emission band is observed at 425 nm.

Luminescence Spectra. In the luminescence spectra of the solid compound **I** (Figure 8), two bands of almost equal

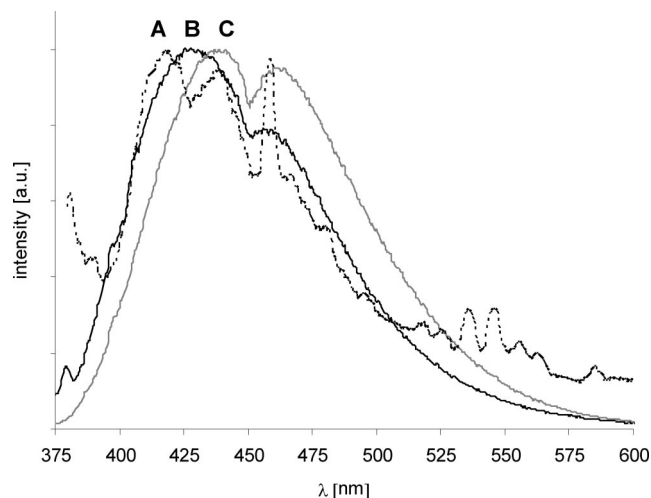


Figure 8. Room temperature emission spectra of **I**: in the solid state, $\lambda_{\text{exc}} = 360$ nm (A); in *n*-PrOH, $\lambda_{\text{exc}} = 359$ nm (B); in acetonitrile, $\lambda_{\text{exc}} = 355$ nm (C).

intensity (425 and 440 nm) and a shoulder at about 470 nm with the vibrational structure (480, 495, 518, 526, 536, 546, 556, 563, and 585 nm) are observed. The longest wavelength broad band with a maximum at about 550 nm seems to be the phosphorescence band that will be the subject of further investigations.

A comparison of the emission spectrum of **I** performed in a less polar *n*-PrOH (dielectric permittivity $\epsilon = 18$) with that in strongly polar acetonitrile ($\epsilon = 37$) shows a significant solvent effect. The corresponding maxima of a double luminescence are at 429 and 460 nm and at 440 and 462 nm, respectively. The Stokes shift values with respect to a longer wavelength band and the intensity ratio of the longer to the shorter wavelength band are larger in acetonitrile (6524 cm^{-1} ; 0.95) than in *n*-PrOH (4550 cm^{-1} ; 0.77). These facts affirm an increase of the excited-state dipole moment of **I** and better stabilization of the excited structure in more polar acetonitrile, which subsequently confirms the CT nature of the emissive state of **I**. As for the copper(II) ion, most probably it is the LMCT state resulting from a shift of charge from electron-donating groups (OCH₃ or OC₂H₅) to the copper(II) ion¹³ and leading as a consequence to its reduction and formation of the copper(I) ion.

The Stokes shift, larger than 6500 cm^{-1} in acetonitrile, is a photophysical parameter that suggests important changes in the nuclear configuration between the ground and excited

(52) Bargeletti, F.; Dellonte, S.; Orlandi, G.; Bartocci, G.; Masetti, F.; Mazzucato, U. *J. Chem. Soc., Faraday Trans. 1* **1984**, *80*, 1123–1129.
(53) Bartocci, G.; Masetti, F.; Mazzucato, U. *J. Chem. Soc., Faraday Trans. 2* **1984**, *80*, 1093–1105.

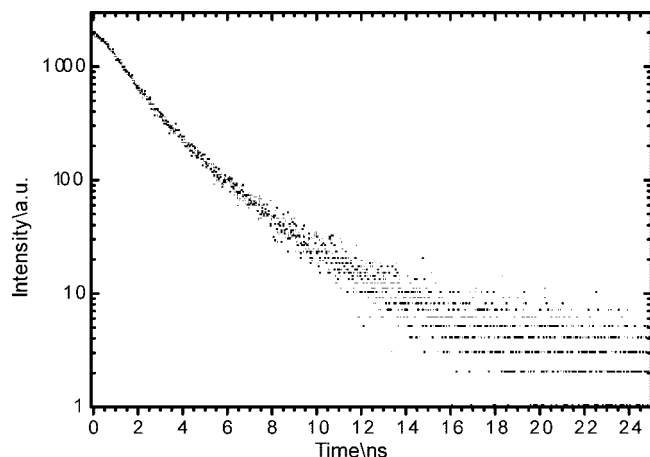


Figure 9. Biexponential decay of **I** in acetonitrile (excitation, 360 nm; emission, 460 nm).

states.⁵⁴ Hence, one may suppose that, because of the possibility of rotation of particular fragments of 4-(4-methoxystyryl)pyridine *N*-oxide moieties around the single C–C bond, both *cis* and *trans* interconverting forms of the styryl moiety may be formed in the excited state, both of them may show the CT nature, and both of them may contribute to the total Stokes shift value.

Lifetimes. A double-bumped emission spectrum of the copper dimer in fluid acetonitrile is broader and more intense than that in rigid (77 K) *n*-propanol. According to the above discussion, one may assign them to different conformers of **I**.

These two excited-state conformers may slightly differ in emission intensity (quantum yield) and have rather similar emission spectra (440 and 462 nm) but greatly different lifetimes. Indeed, room temperature lifetime measurements performed in acetonitrile demonstrate an emissive singlet state and biexponential decay with one major component of 0.8 ns (91%) and the second one substantially longer of about 4.0 ns (9%). Such a biexponential decay curve, as presented in Figure 9, may confirm the existence of two different excited-state CT species of **I**. The corresponding data are displayed in Table 6.

Large values of the Stokes shift (about 6000 cm^{−1}; Table 6) indicate also that we are dealing with a situation where the excited-state potential energy surface and that of the ground state are strongly shifted. Transition from the higher energy curve to the ground-state curve requires a rather small amount of energy and, therefore, a relatively short lifetime is found for the major component.

In frozen *n*-propanol, i.e., in (nonequilibrium) rigid glass structure where the relaxation processes involve microscopic configurations that are structurally slightly different but of a

similar energy, the whole dynamics is slowed down and therefore the elongated lifetimes are observed. The shorter component in acetonitrile (0.8 ns; Table 6) is now about 2 ns, while the longer one (4.12 ns) is now about 15 ns.

It is worthwhile to notice that a different way of deactivation of the excited molecule **I** is observed in the solid where the potential surface minimum is related to the structural order. An effective spin–orbit coupling opens both the intersystem crossing and luminescence channel due to the fact that we are dealing only with the monoexponential decay curve. The estimated lifetime is about 9.0 μs.

Conclusions

(1) The novel mixed adduct of a binuclear complex (1:1) of *N*-oxide and CuCl₂, containing two different extra ligands, water and ethanol, was obtained for the first time, and its X-ray crystal structure has been resolved. The complex **I** consists of binuclear units. Two molecules of dimer **I** form a doubly hydrogen-bonded superdimer in which they are connected to each other by Cl⋯H–O(Et) types of hydrogen bonds between chlorine atoms and an ethanol molecule (Cl⋯O 3.22 Å). The water molecules form hydrogen bonds with CH₃O groups of other dimers (O⋯O 2.761 Å), producing an infinite chain of dimers. In contrast to known complexes, the pyridine rings in complex **I** form a torsion angle of 32.5°.

(2) Very strong antiferromagnetic coupling between copper(II) ions in dimeric units of **I** has been observed on the basis of the large singlet–triplet energy gap ($2J = -1100$ cm^{−1}). It is shown to be substantially larger than the value expected from Hatfield's rule for the bridging Cu–O–Cu angles equal to 108.9° and 110.2°.

(3) Initial studies of photophysical properties were performed by a combination of experimental and PM3 quantum theoretical methods. On this basis, the MLCT and LMCT bands of **I** in unresolved reflectance spectra of a solid and in the absorption spectra in *n*-propanol and acetonitrile were identified.

(4) A significant solvent effect demonstrated by a large value of the Stokes shift in polar acetonitrile (about 6500 cm^{−1}) with respect to a less polar *n*-propanol (about 4500 cm^{−1}) confirms the CT nature of the emissive state (LMCT) of **I**.

(5) Dual fluorescence decay in solution is related to the two separate excited-state CT forms (0.8, 4.12 ns and 1.99, 15.2 ns, in acetonitrile and frozen propanol, respectively), while in the solid, due to the structural order and effective spin–orbit coupling, only the monoexponential decay curve with a lifetime of about 9.0 μs has been observed.

Supporting Information Available: X-ray crystallographic data in CIF format. This material is available free of charge via the Internet at <http://pubs.acs.org>.

IC701413M

(54) Valeur, B. *Molecular Fluorescence: Principles and Application*; Wiley-VCH Verlag GmbH: Weinheim, Germany, 2001.